A Time Series Characterization of IGBT Junction Temperature Method Based on LSTM Network

Zheng-Wei Du, *Student Member, IEEE*, Yu Zhang, Yuankui Wang, Zhiyuan Chen, Yin-Da Wang, *Graduate Student Member, IEEE*, Rui Wu, Dongyan Zhao, *Senior Member, IEEE*, Xin Zhang, *Senior Member, IEEE*, and Wen-Yan Yin, *Fellow, IEEE*

***Abstract*—Accurate junction temperature characterization plays a critical role in the performance as well as reliability enhancement design of Insulated gate bipolar transistor (IGBT) modules. However, most current methods are only focused on predicting the temperature at a specific time rather than tracking its temporal variation. To address this challenging issue, we propose a long short term memory (LSTM) neural network-based method for predicting the junction temperature time series of IGBTs, and it can comprehensively characterize the time-dependent junction temperature according to the measured and validated experimental results. As the convolutional neural network is limited in its ability to remember temporal information, we integrate the LSTM networks for training, which can fast capture long-time dependencies in the data. Therefore, we exploit the superior performance of LSTM network for predicting the junction temperature of IGBTs here. It is shown that there is a strong correlation between the maximum junction temperature of IGBT and its parameters, such as bus voltage, load current, carrier, and output frequencies, as well as its heat sink parameters. By leveraging the LSTM-based method, an accurate time series information of the junction temperature is successfully captured under different operating conditions. Notably, in comparison with the current machine learning method, the proposed method can outperform in the same training dataset.**

Received 11 March 2024; revised 17 May 2024 and 6 August 2024; accepted 8 September 2024. Date of publication 12 September 2024; date of current version 12 December 2024. This work was supported in part by the National Natural Science Foundation of China under Grant U23A20350 and in part by the Laboratory Specialized Scientific Research Projects of Beijing Smart-Chip Microelectronics Technology Company, Ltd., of China under Grant SGSCD-TOOYFQT24 00749. Recommended for publication by Associate Editor C. DiMarino. *(Corresponding author: Wen-Yan Yin.)*

Zheng-Wei Du, Yu Zhang, Zhiyuan Chen, Yin-Da Wang, and Wen-Yan Yin are with the Innovative Institute of Electromagnetic Information and Electronic Integration, Zhejiang University, Hangzhou 310027, China, and also with the Key Lab of Advanced Micro-Nano Electronic Devices and Smart Systems of Zhejiang Province, College of Information Science and Electronic Engineering, Zhejiang University, Hangzhou 310027, China (e-mail: wyyin@zju.edu.cn).

Yuankui Wang is with the Ocean College, Zhejiang University, Zhejiang 316021, China, and also with the China State Shipbuilding Company, Ltd., Kunming 650000, China.

Rui Wu is with the Zhejiang Grecon Semiconductor Company, Ltd., Shanghai 201210, China, and also with the College of Automation Engineering, Nanjing University of Aeronautics and Astronautics, Nanjing 211106, China.

Dongyan Zhao is with the Beijing Smart-Chip Microelectronics Technology Company Ltd., Beijing 100192, China, and also with the International College, Zhejiang University, Zhejiang 310058, China.

Xin Zhang is with the School of Electrical Engineering, Zhejiang University, Hangzhou 310027, China.

Color versions of one or more figures in this article are available at https://doi.org/10.1109/TPEL.2024.3459470.

Digital Object Identifier 10.1109/TPEL.2024.3459470

***Index Terms*—Insulated-gate bipolar transistor (IGBT), long short term memory (LSTM), maximum junction temperature, parameter dependence.**

I. Introduction

INSULATED gate bipolar transistors (IGBTs) have been widely used in various power electronic systems, due to their high power densities, high efficiencies, fast switching speeds, and flexible controls [1]. On the other hand, it is well known that the fluctuation of junction temperature in an IGBT does affect its operation performance [2], [3]. While the junction temperature prediction of an IGBT can detect its potential operating problems in advance. That is the main motivation behind this research.

In general, there are four main approaches for obtaining the junction temperature of IGBT modules: 1) direct device measurement, 2) thermal model method, 3) temperature sensing based on electrical parameters, and 4) prediction using machine learning (ML) or artificial intelligence (AI) algorithm. In the first approach, as shown in [4], it employs an infrared thermal camera to directly measure the junction temperature of the IGBT module. The junction temperature can be determined by analyzing the phase difference of the heat wave and optical modulation [5]. Direct methods for detecting the junction temperature include the use of a fiber-optic temperature sensor [6] and a thermocouple [7], which involve physical contact with the IGBT. In [8], the estimation of junction temperature is performed by monitoring the negative temperature coefficient (NTC) resistor within the IGBT. On the other hand, an online estimation system based on the NTC method is developed in [9]. These methods necessitate precise measurement devices for achieving accurate results. The unpacking of an IGBT, insertion of foreign matter and requirements of high-accuracy devices make its junction temperature acquisition intricate and high-cost.

As for the thermal model method, Cauer and Foster thermal networks are commonly utilized. For example, thermal networks with a 1-D structure have been established in the previous studies [10], [11], [12], [13], such as lumped parameter thermal network [14]. The 2-D thermal networks have also been proposed in [15], [16], and [17], respectively, taking surface thermal parameters into consideration. Furthermore, 3-D thermal networks have

been developed as presented in [18], [19], [20], and [21], respectively, which take into account both the vertical and horizontal propagation of heat. On the other hand, in order to obtain the thermal field distribution in an IGBT, well popular finite element method [22], has often been employed to create cooling curves of the junction temperature [23], transient temperature curves in different layers [24], and transient thermal impedance curves [25], [26]. In addition, some analytical methods have been proposed for fast solving the heat-transfer equation utilizing the Green's function and Fourier series so as to fast obtain the temperature data [27], [28], [29].

The third approach involves estimating the junction temperature using temperature-sensitive parameters [30], including static as well as dynamic parameters. The static parameters include forward voltage drop [31], [32], short-circuit current [33], [34], gate voltage [35], and flatband voltage [36]. The dynamic parameters include turn-ON or turn-OFF delay time [37], [38], collector voltage change rate during turn-OFF [39], and turn-OFF voltage [40]. These methods can be employed to analysis of the relationship between the device parameters and its junction temperature for further predicting the thermal effects.

The fourth approach to utilize ML and AI algorithms for fast characterization of junction temperature of an IGBT. In the previous studies, several AI algorithms have been developed to estimate the working conditions and parameters of IGBTs, as demonstrated in [41] and [42], respectively, where multiple parameters were combined to train the neural networks (NNs) in [43]. While in [44] and [45], NNs are trained with different parameters, such as conductions and gate voltages to estimate the junction temperature of an IGBT, respectively. In [40], the junction temperature is predicated based on a convolutional neural network (CNN) using the shut-OFF voltage values, while the other method for temperature prediction is performed, but without considering wire bond degradation [46]. Indeed, these current ML and AI methods can be effectively employed for predicting the junction temperature at a specific moment, but they do not consider the junction temperature changes over certain time.

We also would like to emphasize that the current ML and AI methods are often used for predicting the junction temperature. However, it is only suitable for single-point prediction, and it lacks the capability for time series cases. To address this limitation, it is known that long short-term memory (LSTM) deep learning network can predict the junction temperature of IGBT with time variation. It incorporates a feedback mechanism, and it is commonly used in semantic recognition, medical signal recognition [47], and communication signal prediction and recognition [48], [49]. In comparison with the existing prediction algorithms, such as CNN, decision trees, and particle swarm optimization, LSTM demonstrates its superior performance for forecasting the IGBT time series, due to its ability for capturing temporal sequence characteristics [50], [51].

Therefore, this article presents an IGBT junction temperature time series prediction method based on the LSTM network, where the prediction of a complete time series enables a comprehensive reflection of the temperature changes in the IGBT.

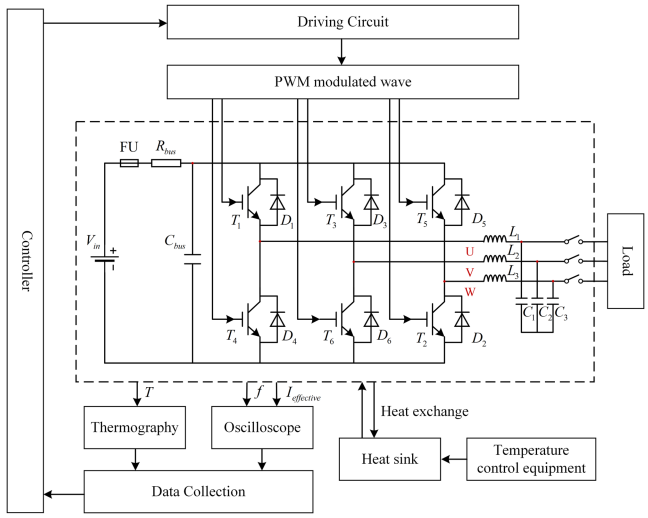

Fig. 1. IGBT operation circuit diagram.

The prediction of the junction temperature of an IGBT without direct observation can serve as a fundamental element for the thermal management design of most power electronics modules. Through online IGBT prediction, anticipatory detection of potential operational faults becomes viable, thereby facilitating technical assistance for the advancement of IGBT digital twin technology aimed at achieving synchronization between actual system parameters and their digital counterparts. Additionally, before training, we analyze and prioritize experimentally obtainable parameters for the IGBT, examine the dependence of the IGBT junction temperature on each parameter, and verify the results through experiments. This method offers the advantages, such as easy application in engineering practice, prediction of continuous temperature sequences, and high accuracy.

The rest of this article is organized as follows. In Section II, the IGBT junction temperature affecting factors are described. Furthermore, the principles of the LSTM network are explained in Section III. In Section IV, the IGBT junction temperature parameter dependence verification experiment is performed. In Section V, the analysis of the predicted junction temperature is carried out. Finally, Section VI concludes this article.

II. Analysis of IGBT Junction Temperature Affecting Factors

To predict the junction temperature of IGBTs requires a comprehensive analysis of its affecting factors. The careful selection of independent parameters for predicting the junction temperature plays a crucial role in enhancing the accuracy of NN training. The high junction temperature of IGBT is mainly contributed by its power loss, working environment, heat dissipation conditions, and power supply fluctuations. We choose one operating circuit of IGBT, i.e., a three-phase inverter system, as an example plotted in Fig. 1, to show the parameter effects on the junction temperature of IGBT.

Such a UVW three-phase inverter circuit comprises six groups of IGBTs and a set of Freewheeling diodes (FWDs), with a phase

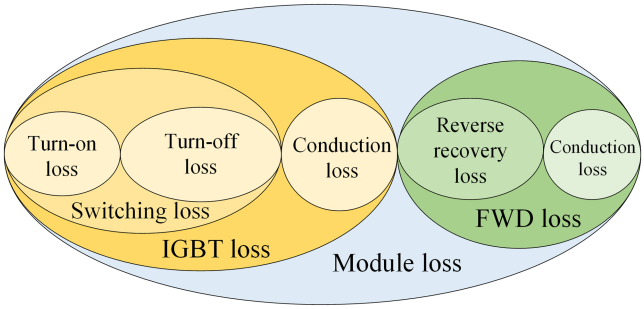

Fig. 2. Diagram of subordinate relationship of an IGBT module loss.

difference of 60° between the current and voltage waveforms in each group.

The module loss during operation is primarily categorized as IGBT loss $P_{\mathrm{IGBT,loss}}$ and FWD loss $P_{\mathrm{FWD,loss}}$. IGBT loss is further categorized into conduction loss $P_{\mathrm{IGBT,cond}}$ and switching loss $P_{\mathrm{IGBT,sw}}$, with switching loss being further divided into turn-ON loss $P_{\mathrm{IGBT,on}}$ and turn-OFF loss $P_{\mathrm{IGBT,off}}$. The FWD loss is divided into conduction loss $P_{\mathrm{FWD,cond}}$ and reverse recovery loss $P_{\mathrm{FWD,rec}}$. For ease of analysis, it is assumed that the load current $I_c(t)$ and the voltage of collector-emitter port $V_{ce}(t)$ remains relatively constant within a switching period t_{sw}. The attribution relationship of each loss is illustrated in Fig. 2. For the IGBT conduction loss, we have

$$\begin{aligned} P_{\mathrm{IGBT,cond}} &= \frac{1}{t_{sw}} \int_{t_1}^{t_2} V_{ce}(t) I_c(t) \mathrm{d}t \\ &= V_{ce} I_c \frac{t_2 - t_1}{t_{sw}} = V_{ce} I_c \delta \end{aligned} \tag{1}$$

where δ is the duty ratio, and $V_{ce}(t)$ is calculate by

$$V_{ce} = V_{ce0} + I_c r_{ce} \tag{2}$$

where V_{ce0} is the initial saturation voltage drop, and r_{ce} is the ON-resistance. According to the output characteristic curve in the IGBT technical manual, both V_{ce0} and r_{ce} can be fitted as

$$V_{ce0} = V_{ce0,25} + k_{\mathrm{IGBT},v}(T_j - 25^\circ C) \tag{3}$$

$$r_{ce} = r_{ec,25} + k_{\mathrm{IGBT},r}(T_j - 25^\circ C) \tag{4}$$

where $V_{ce0,25}$ and r_{ce} are the initial saturation voltage drop and ON-resistance at the junction temperature of 25°C, respectively. $k_{\mathrm{IGBT},V}$ and $k_{\mathrm{IGBT},r}$ are the temperature correction coefficient, and T_j is the junction temperature.

The other important factor affecting the conduction loss is the duty ratio. In the SPWM modulation, the sine wave expression is described by $U_{\mathrm{smax}} \cdot \sin(\omega t)$, the triangle wave amplitude is U_{cmax}, and the period is t_{sw}. Assuming that the sine wave amplitude of IGBT primary switching time is a constant approximately, and it can be expressed as

$$\frac{t_2 - t_1}{U_{\mathrm{cmax}} + U_{\mathrm{smax}} \cdot \sin(\omega(t_2 - t_1))} = \frac{t_{sw}}{2U_{\mathrm{cmax}}} \tag{5}$$

where t_1 and t_2 denote the turn-ON and turn-OFF time of IGBT primary switch, respectively. Then, the duty ratio can be expressed as

$$\begin{aligned} \delta(t) &= \frac{t_2 - t_1}{t_{sw}} = \frac{1 + U_{\mathrm{cmax}}/U_{\mathrm{smax}} \cdot \sin(\omega t)}{2} \\ &= \frac{1 + m \sin(\omega t)}{2} \end{aligned} \tag{6}$$

where m is the degree of modulation, and it can be calculated as $m = U_{\mathrm{cmax}}/U_{\mathrm{smax}}$. The conduction loss of IGBT can be deduced as

$$\begin{aligned} &P_{\mathrm{IGBT,cond}} = \\ &I_c \left[V_{ce0,25} + k_{\mathrm{IGBT},V}(T_j - 25^\circ \mathrm{C})\right] \frac{1 + m \sin(\omega t)}{2} \\ &+ {I_c}^2 \left[r_{ce,25} + k_{\mathrm{IGBT},r}(T_j - 25^\circ \mathrm{C})\right] \frac{1 + m \sin(\omega t)}{2}. \end{aligned} \tag{7}$$

According to the same steps, the conduction loss of FWD $P_{\mathrm{FWD,loss}}$ can be calculated, which is mainly related to the load current, bus voltage, output waveform frequency, junction temperature, modulation degree, saturation conduction voltage drop, and conduction resistance.

The switching loss of IGBT can be obtained by fitting the switching loss curve in the technical manual. By adding different correction coefficients, the loss calculation can be more accurate. While the switching loss of IGBT can be expressed as

$$\begin{aligned} P_{\mathrm{IGBT,sw}} &= P_{\mathrm{IGBT,on}} + P_{\mathrm{IGBT,off}} = f_{sw} E_{sw} k_V k_R k_T \\ &= f_{sw}(A_{sw} {I_c}^{B_{sw}}) \left(\frac{V_{\mathrm{dc}}}{V_{\mathrm{dc,base}}}\right)^{n_{V_{dc}}} \left(\frac{R_{\mathrm{g}}}{R_{\mathrm{g,base}}}\right)^{n_{R_g}} \\ &\quad \times \left[1 + n_T \left(T_j - T_{j,\mathrm{base}}\right)\right] \end{aligned} \tag{8}$$

where f_{sw} is the frequency of carrier signal and E_{sw} is the fitting expression based on the technical manual data. k_V is the voltage correction factor, k_R is the resistance correction factor, and k_T is the temperature correction factor. A_{sw} and B_{sw} are the fitting expression coefficient. V_{dc} is the bus voltage, R_{g} is the gate resistance, T_j is the junction temperature, and $V_{\mathrm{dc,base}}$, $R_{\mathrm{g,base}}$, and $T_{j,\mathrm{base}}$ are the reference values in the manual, respectively. $n_{V_{dc}}$, n_{R_g}, and n_T are the correction coefficients, respectively. The reverse recovery loss of the FWD can be calculated by the above method. The switch loss is mainly related to load current, bus voltage, switching frequency, gate resistance, and junction temperature.

In order to predict the junction temperature accurately, some researchers often employ one thermal resistance network to simulate the thermal effects in IGBT. With only the vertical heat conduction within the IGBT module considered, the thermal resistance network can be derived by assessing the system power consumption, as depicted in Fig. 3.

Within an entire heat dissipation circuit, both IGBT and FWD serve as heat sources, with heat being transferred to the substrate through DBC and dissipated by coolant. In the diagram, the heat dissipation capacity between the substrate and environment varies based on the coolant temperature and flow rate, effectively

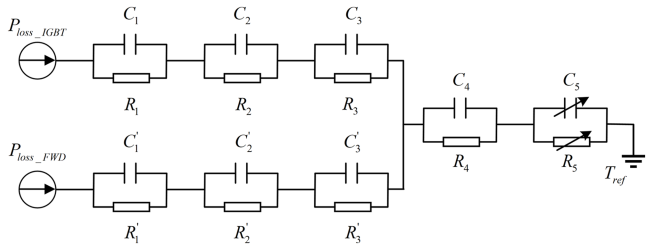

Fig. 3. Thermal resistance model of the IGBT operating circuit.

resembling variable thermal resistance and heat capacity. The heat dissipation in the coolant can be described by the fluid equation as

$$\rho C_\rho \frac{\partial T}{\partial t} + \rho C_\rho \overrightarrow{u} \cdot \nabla T + \nabla \cdot \overrightarrow{q} = Q \tag{9}$$

where ρ is the fluid density, C_ρ is the heat capacity, $\overrightarrow{u}$ is the fluid velocity, Q is the heat source, and the heat flux $\overrightarrow{q}$ is described by

$$\overrightarrow{q} = -k\nabla T \tag{10}$$

where k is the thermal conductivity. When the coolant temperature in the water tank is increased, the temperature difference between the coolant flow and the heat dissipation is reduced. Therefore, the heat dissipation through the water flow is reduced, while the junction temperature will be increased. Based on the aforementioned analysis, the input parameters for the NN prediction should include carrier frequency, load current, bus voltage, output frequency, and IGBT heat sink related parameters, which includes water temperature, water pressure, and water flow velocity in the IGBT heat sink channel.

III. Feature Information Extraction Method Based on Long Short-Term Memory Network

A. Feedback Neural Network

Unlike the feedforward neural networks, feedback neural networks (FBNN) allow neurons to not only receive the signals from the other neurons but also receive the feedback signals from their own previous states. This memory function of FBNN enables it to process continuous information with temporal characteristics effectively.

The recurrent neural network (RNN) is the most representative type of FBNN, incorporating self-feedback loops and repetition to retain characteristic information over time [52], [53]. It has high efficiency in handling time series data, extracting timing, and semantic information from training data effectively [54]. However, it faces two significant challenges, as the length of time series increases. At first, the front layers in the RNN stop updating parameters effectively, as the learning rate decreases during training, indicating that RNN possesses only short-term memory. Second, it suffers from the gradient explosion with the number of training layers, which is attributed to the backpropagation training rule with a large number of chain derivatives.

To address the issues of gradient vanishing and explosion in RNN, the LSTM network has been developed [48]. It employs a different framework than that of the RNN for calculating the hidden layer states, thus overcoming the problems associated with long-term time series information [55]. Therefore, the LSTM network is utilized for predicting the junction temperature time series, as it offers better training effects compared to RNN.

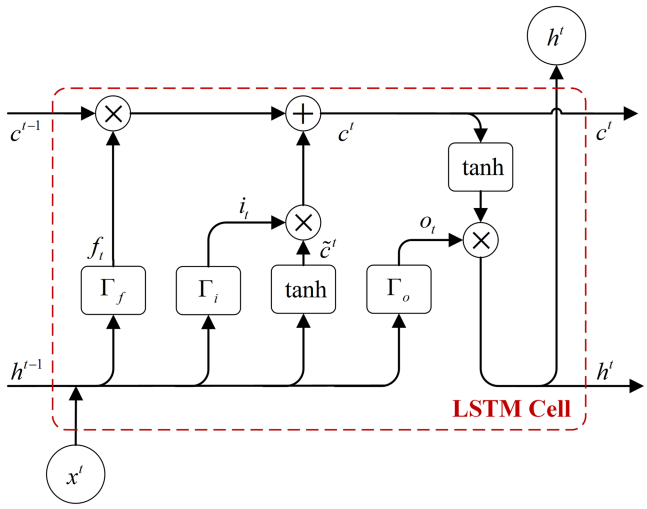

Fig. 4. Structure of the LSTM cell.

B. Structure of LSTM

LSTM has a chain network structure that repeats the NN module, and it is called the LSTM cell. The LSTM cell has three independent inputs: at the time t network input variablex^t, at the time $t-1$ the LSTM output value h^{t-1}, and the time$t-1$ LSTM cell state c^{t-1}. Correspondingly, at the time$t$ LSTM output variableh^t, and at the time t LSTM cell state c^t is used as the cell outputs. The detailed of LSTM cell is shown in Fig. 4.

Such LSTM has three types of gate structures: 1) forgetting, 2) input, and 3) output gates for protecting and controlling the cell states. The forgetting gate Γ_f determines what information should be discarded from the cellular state, where nonlinear mapping is applied to filter the important features in the forgetting gate. Then, the output vectorf_t affects the cell state update, and the vector f_t can be obtained by

$$f_t = \Gamma_f(x^t, h^{t-1}) = \sigma\left(W_f \cdot \begin{bmatrix} x^t \\ h^{t-1} \end{bmatrix} + b_f\right) \tag{11}$$

where W_f and b_f are two training parameters of the network, but W_f is not the common parameter for x^t and h^t, and $\sigma(\cdot)$ is the nonlinear mapping function.

The input gate determines, which new information should be stored in the cell state. Similar to the forgetting gate, the sigmoid activation function and the weight parameter are used to select valuable features at the input gate, as given by

$$i_t = \Gamma_i(x^t, h^{t-1}) = \sigma\left(W_i \cdot \begin{bmatrix} x^t \\ h^{t-1} \end{bmatrix} + b_i\right) \tag{12}$$

where W_i and b_i are two training parameters of the network, and the update process is the same as above. The state of cell c^t is

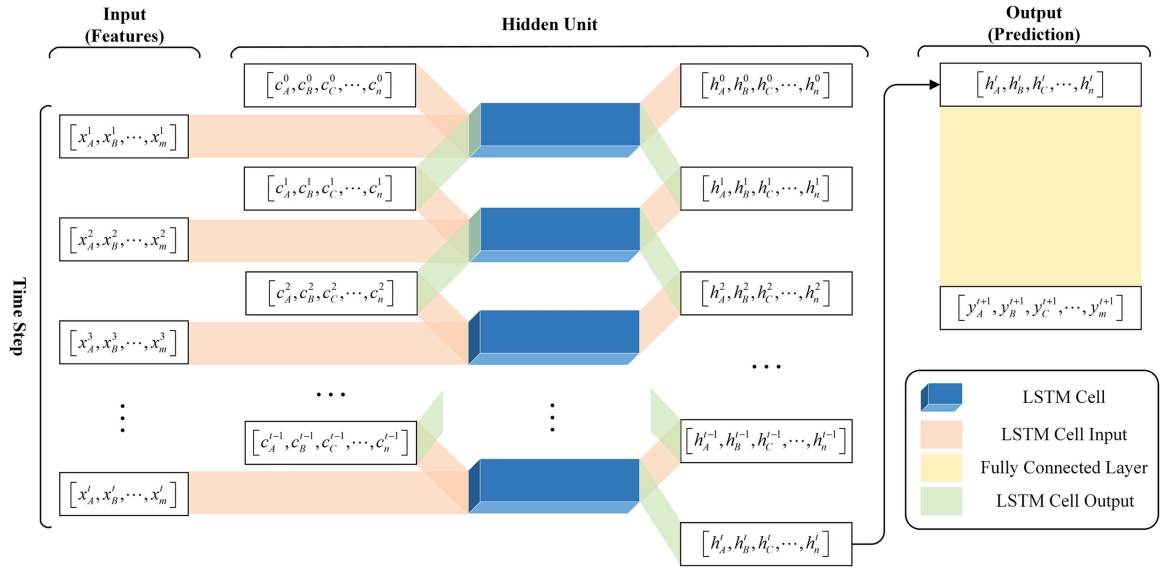

Fig. 5. Operation mechanism of LSTM network.

calculated by forgetting and input gates, respectively, and

$$c^t = \left[\Gamma_f\left(x^t, h^{t-1}\right) \otimes c^{t-1}\right] \oplus \left[\Gamma_i\left(x^t, h^{t-1}\right) \otimes \tilde{c}^t\right] \tag{13}$$

where $\otimes$ represents the multiplication of the corresponding elements in the matrix, $\oplus$ denotes the corresponding elements addition, $\tilde{c}^t$is the candidate of LSTM cell state, and

$$\tilde{c}^t = \tanh\left(W_c \cdot \begin{bmatrix} x^t \\ h^{t-1} \end{bmatrix} + b_c\right) \tag{14}$$

where W_c and b_c are two training parameters, and $\tanh(\cdot)$ is the nonlinear mapping function.

The output gate determines what value should be sent to output, which is based on the cell state. Meanwhile, the output of the previous cell will also be considered. The cell output h^t can be deduced as

$$h^t = \tanh(c^t) \otimes \Gamma_o(x^t, h^{t-1}) \tag{15}$$

and the output gate is written as

$$o_t = \Gamma_o(x^t, h^{t-1}) = \sigma\left(W_o \cdot \begin{bmatrix} x^t \\ h^{t-1} \end{bmatrix} + b_o\right) \tag{16}$$

where W_o and b_o are two training parameters.

Feature extraction of the training target is controlled and is affected by the state of the cell control gate, where long-term information can be remembered, and inessential one can be forgotten. Compared with RNN, the LSTM network has better performance in the long-term memory tasks. Especially, the interior of the LSTM network consists of multiple cell splices, and the connected layers are used at the input and output of the LSTM cell.

The architecture of the network is shown in Fig. 5, with the forward propagation process in the network demonstrated. The input of the network at each step is given by $[c_A^{t-1}, c_B^{t-1}, c_C^{t-1}, \cdots c_m^{t-1}]$, and the $[x_A^1, x_B^1, x_C^1, \cdots x_m^1]$ denotes the number of the mth input features expressed by $x_A, x_B, x_C, \cdots x_m$. In the hidden unit, there are the LSTM cell states at $t-1$, where $[h_A^{t-1}, h_B^{t-1}, h_C^{t-1}, \cdots h_m^{t-1}]$is the LSTM cell output at $t-1$, and m is the number of LSTM cell. All features are linked to the LSTM cells using a fully connected layer. It should be noted that $[c_A^0, c_B^0, c_C^0, \cdots c_m^0]$ and $[h_A^0, h_B^0, h_C^0, \cdots h_m^0]$ need to be initialized before network training. Finally, the fully connected layer is used to transform the LSTM cell output into the network output. Admittedly, there are multiple control gate structures introduced into such LSTM network. It leads to more parameters and makes the training to be more difficult. So, the LSTM network training is very time consuming.

C. Architecture of Time Series Prediction

Early attempts were made to predict the single point junction temperature of IGBT. Here, the LSTM network is used as the feature extraction for predicting the IGBT junction temperature time series. It is worth mentioning that the other parameters can be obtained in a convenient way.

Fig. 6 illustrates the flowchart for predicting the IGBT temperature time series based on the LSTM network, where both experimental test and theoretical analysis are conducted. The IGBT thermal data are collected in our static experiment. Practically, the maximum junction temperature is a significant index to observe the stable operation of IGBT. Its long-term high temperature operation will lead to the aging of solder layer and bonding wire. Therefore, its maximum junction temperature time series prediction is very important for large scale IGBT applications. The full maximum junction temperature waveform is regarded as the inputs, and the temperature data is filtered and regularized.

The effects of different parameters are examined according to the equivalent IGBT module circuit. More easily available parameters are selected to explore the IGBT heating effect. In particular, load current, direct current side bus voltage, driver carrier frequency, output electrical frequency, and the IGBT heat

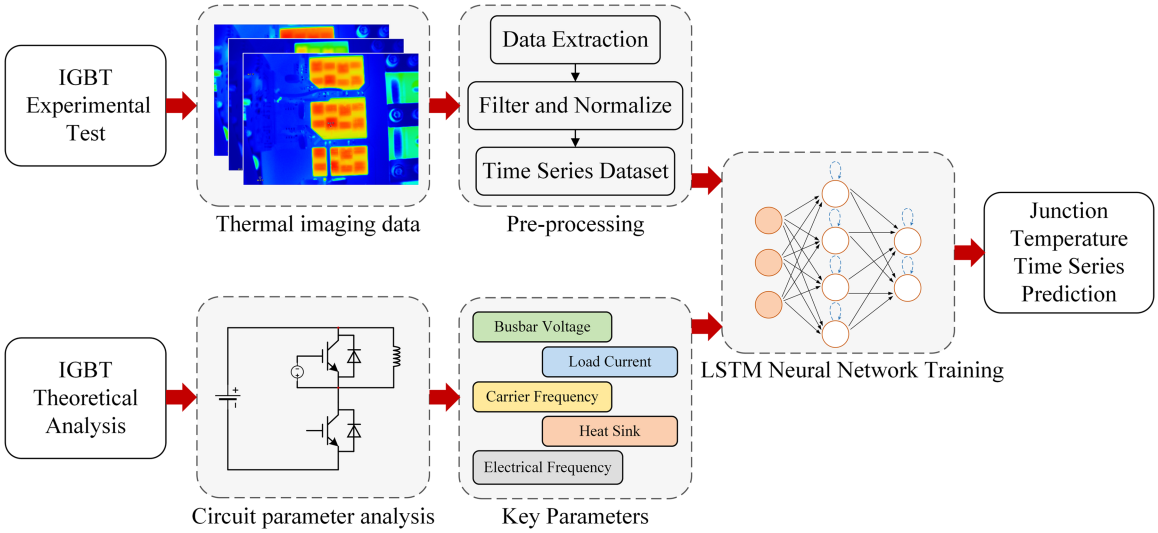

Fig. 6. Flowchart for predicting the IGBT temperature time series.

sink parameters are considered here. Based on theoretical analysis, the parameter-dependence of each parameter is tested and examined, and all key parameters are selected by our analysis and experiment, which is beneficial for the NN training.

As mentioned above, such LSTM network has better performance for the long time series prediction. Here, both training parameters and training data are treated carefully so as to achieve better results. The junction temperature characteristics of IGBT are extracted by using different nonlinear mapping functions in the LSTM network. The full connection layer is used for network feature transmission, and the NN back propagation updates and iterates the network parameters. Through the LSTM network training, our expected IGBT junction temperature time series can be predicted accurately. Furthermore, the network can be trained by the CPU to obtain the parameters of each hidden layer, and it can be loaded onto the MCU to implement the monitoring function.

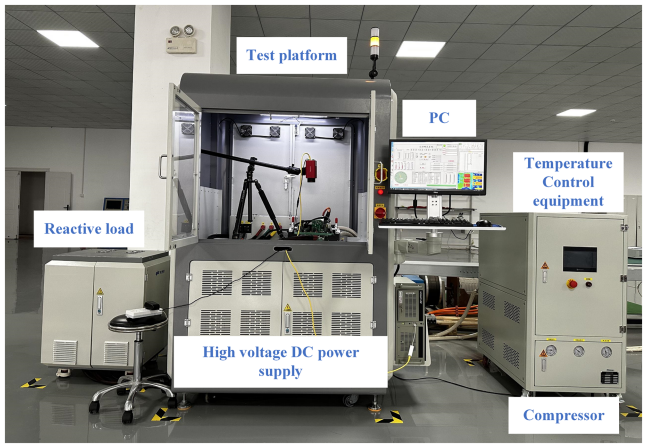

Fig. 7. Photograph of the experimental test bench.

IV. Parameter Dependence Experiment of IGBT Junction Temperature

Building upon the analysis of affecting factors of IGBT junction temperature outlined in Section II, this chapter focuses on the experimental validation, and it is affirmed that each parameter exerts an independent influence on the junction temperature.

A. Experimental Test Bench

Fig. 7 depicts the experimental platform utilized for this study, while Fig. 8 provides a detailed illustration of the internal test platform, which exhibits the electrical connections corresponding to the circuit displayed in Fig. 1. The reactive load employed in the experiment is capable of withstanding the maximum current of 1000 A and the voltage of 500 V. The driving circuit consists of two separate resistors $R_{\mathrm{IGBT(on)}}$ and $R_{\mathrm{IGBT(off)}}$, for

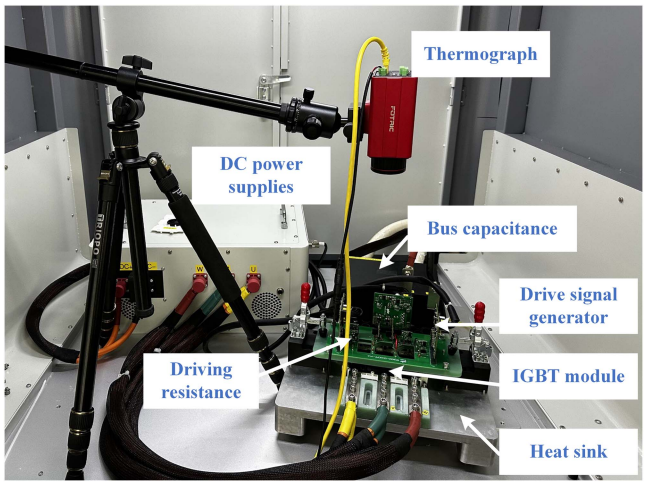

Fig. 8. Photograph of the internal test platform.

TABLE I
INSTRUMENT AND TYPE OF EXPERIMENT PLATFORM

Instruments	Types
Thermograph	Fotric-616C
Bus capacitance	DC1100V-750μF
Data processor	IPC-610-L
Drive signal generator	RP8060-DC6iCPP
Temperature control equipment	JW-10KW-24R
IGBT module	GCV560GT75FTH5H
Test platform	RP8060-FA
DC power supply	YLC072304023

turn-ON and turn-OFF operations, respectively. Both resistances are chosen to be 6 and 12 Ω, respectively.

In order to control the junction temperature of the IGBT, the experimental platform incorporates a heat sink and temperature control equipment. In addition, a thermograph is employed to capture the temporal evolution of the IGBT temperature field. It is important to note that the ambient temperature should be maintained at a stable level, and the heat sink must be implemented throughout the experiment.

In the static test of the IGBT, the voltage and current of the device under test (DUT) can be adjusted within a wide range. Here, the DUT used is the GCV560GT75FTH5H model manufactured by the GRECON-semi. A dedicated test platform is constructed to validate the proposed method for estimating the IGBT junction temperature. The specific information regarding the experimental instruments employed, along with their types, is summarized in Table I.

The selection of training parameters has direct impact on the training performance of NN. Here, we validate the relationship among load current, direct current side bus voltage, driver carrier frequency, output electrical frequency, heat sink-related parameters, and IGBT junction temperature through experiments. The parameter-dependence analysis is conducted using the method of control variables. The temperature curves are obtained from the thermal field distribution videos of IGBT static experiments, where the IGBT module is subjected to various operating conditions until it reaches its stable state.

B. Effect of Load Current and Bus Voltage on IGBT Junction Temperature

The IGBT Module GCV560GT75FTH5H is subjected to testing. The correlation between bus voltage and junction temperature is examined, where the load current of 100 A, the driver carrier frequency of 11.5 kHz, the output electrical frequency of 66 Hz, and the varying direct current side bus voltages of 380, 420, and 460 V are maintained, respectively. The pertinent parameters of the system heat sink, including water tank temperature, flow channel pressure, heat dissipation liquid flow rate are remained to be constant, and one thermal imaging video is captured. To investigate the dependence between bus voltage and junction temperature, we analyze the recorded video and plot the curves of time and junction temperature, with the highest junction temperature selected and depicted in Fig. 9.

The results depicted in Fig. 9 clearly indicate a significant increase in the highest junction temperature with the bus voltage

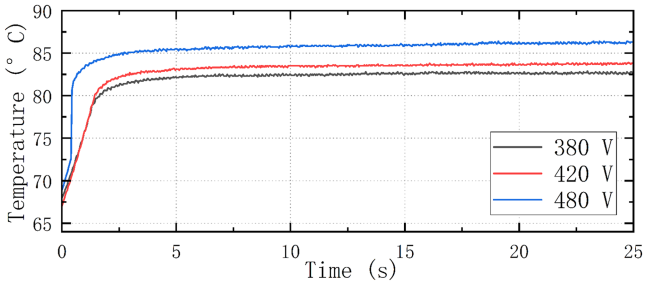

Fig. 9. Effect of bus voltage on the highest junction temperature.

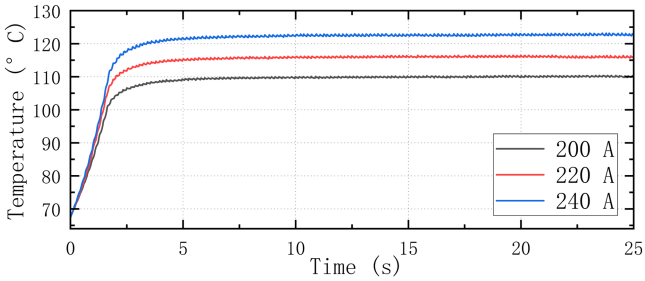

Fig. 10. Effect of load current on the highest junction temperature.

increasing. These findings provide one strong evidence of the strong correlation between the bus voltage and junction temperature. On the other hand, we would like to indicate that these results agree with the theoretical ones in Section II.

As illustrated in Fig. 10, it is evident that the junction temperature escalates with an increase in load current, when the other parameters and conditions remain the same. These experimental findings emphasize the significant impact of bus voltage and load current on the junction temperature. Both the maximum and the overall junction temperature of IGBT module are affected by these factors.

C. Effect of Driver Carrier Frequency and Electrical Frequency on Junction Temperature

The IGBT Module GCV560GT75FTH5H is subjected to testing. In this section, the driver carrier and output electrical frequencies are investigated. To study the effect of the driver carrier frequency, two different operating conditions of the IGBT module are employed as dependent variables in the experimental setup. Specifically, the direct current side bus voltage is set to 480 V, the load current is set at 100 and 200 A, respectively. An output electrical frequency of 66 Hz, and varying driver carrier frequencies of 10.0, 11.0, and 11.5 kHz, respectively. Therefore, changes in junction temperature under these different working conditions are recorded, with the highest junction temperature plotted against time in Fig. 11.

In Fig. 11, it is observed that the IGBT junction temperature increases with the rise in the control signal carrier frequency gradually, while keeping the load current constant. This observation further supports the findings in the previous section, which indicates the load current effect on the junction temperature.

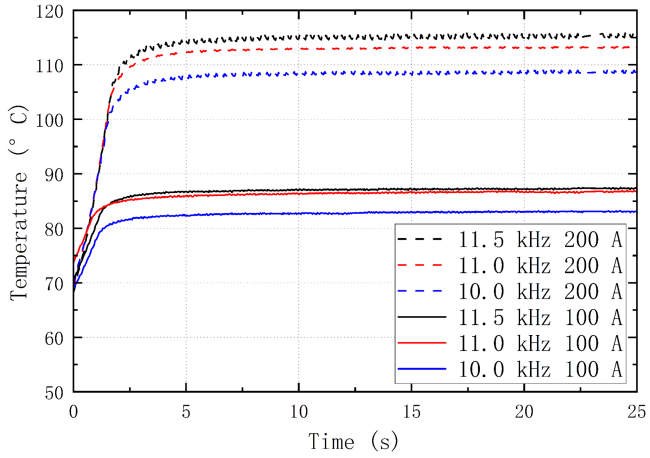

Fig. 11. Effect of the carrier frequency on the highest junction temperature.

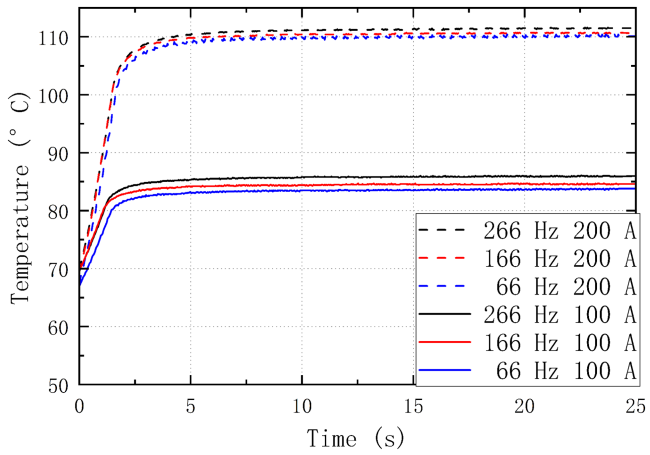

Fig. 12. Effect of the electrical frequency on the highest junction temperature.

Notably, as depicted in Fig. 11, the junction temperature is additionally impacted by the carrier frequency. Thus, it can be deduced that the effects of carrier frequency and load current on the junction temperature are relatively independent variables. These factors should be taken into account during network training.

Similarly, the test for output electrical frequency is conducted, the direct current side bus voltage is set at 420 V, the load current is maintained at 100 and 200 A, respectively. The driver carrier frequency is fixed at 11.5 kHz, and the output electrical frequency is varied as 66, 166, and 266 Hz, respectively. The highest junction temperature is monitored over the whole time, as shown in Fig. 12. Similar to the aforementioned analysis, the output electrical frequency can also affect the junction temperature of IGBT module, building upon the effect of load current.

D. Effect of Heat Sink on Junction Temperature

In addition to the aforementioned parameters, it is important to consider the heat sink conditions during the operation of the IGBT module, as they have significant impact on the junction temperature. The heat sink plays a crucial role in cooling the circulating water during operation. Since the water has a high specific heat capacity, and its temperature in the heat sink does not remain stable at a fixed value. Consequently, the operating parameters of the heat sink also affect the junction temperature of IGBT module.

TABLE II
HEAT SINK PARAMETERS UNDER DIFFERENT IGBT WORKING CONDITIONS

Condition number	Maximum junction temperature (°C)	Water tank temperature (°C)	Heat sink flow (L/Min)	Average heat sink temperature (°C)	Heat sink pressure (kPa)
1	104.4	60	7.6	58.74	69
2	110.4	66	7.7	64.91	69
3	114.4	70	7.6	68.95	68

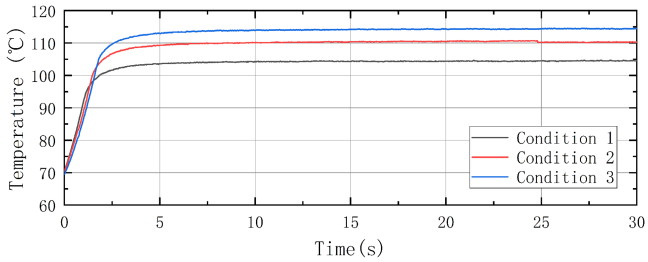

Fig. 13. Effect of the heat sink on the highest junction temperature.

The experiment was conducted under specific operating conditions, with the bus voltage of 420 V, the load current of 100 A, the driver carrier frequency of 11.5 kHz, and the output electrical frequency of 66 Hz. Three experiments were performed, and various thermal variables including the maximum junction temperature, water tank temperature, heat sink flow, average heat sink temperature, and heat sink pressure were recorded and summarized in Table II.

The time-dependent curve of the maximum junction temperature is presented in Fig. 13, with the results of three different operating conditions shown. It can be observed that there is only a slight variation in the maximum junction temperature for different heat sink parameters, which is consistent with the theoretical analysis presented in the previous chapter. To further analyze the effect of heat sink parameters on the overall temperature of IGBT module, the temperature distribution of the IGBT module on the higher temperature side was recorded, when the junction temperature reached its maximum. The temperature distributions under three different working conditions are illustrated in Figs. 14, 15, and 16, respectively.

By comparing Figs. 14, 15, and 16, it can be observed that the spatial distribution of the IGBT junction temperature remains essentially unchanged, while the overall junction temperature varies. This implies that the heat sink parameters do not significantly affect the distribution of the junction temperature, but has rather impact on the level of the junction temperature. These findings hold significant reference value for the subsequent deep learning training below.

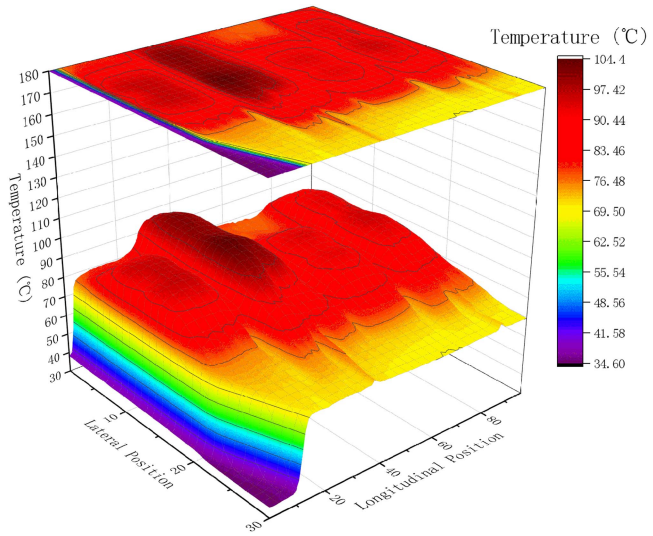

Fig. 14. IGBT junction temperature distribution under Condition 1.

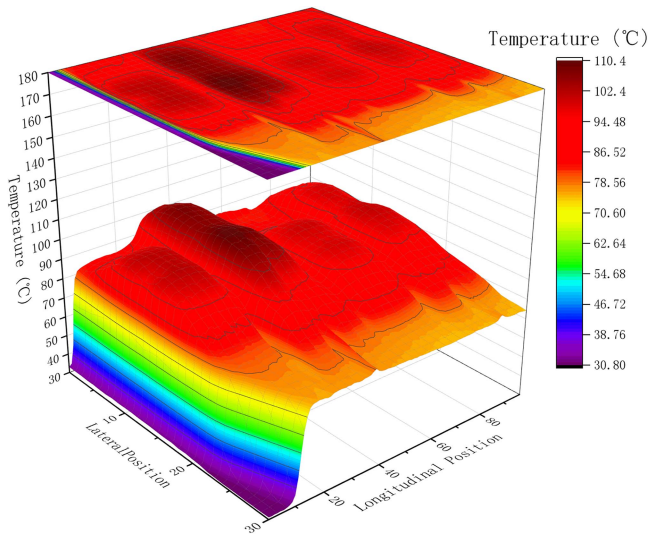

Fig. 15. IGBT junction temperature distribution under Condition 2.

E. Effect of Module Aging on Junction Temperature

In the power cycle experiment of the IGBT module, its aging effects results in an increased thermal resistance, and consequently, raises its maximum junction temperature. Therefore, the junction temperature varies among the IGBT chips with different degrees of aging under identical operational conditions. However, upon testing the saturation conduction voltage drop across all IGBT chips discussed in this study, significant variations were observed in the saturation voltage drop between the chips. Not only do the six IGBT chips within a module exhibit disparity, but also chips within an identical IGBT module manifests significant differences. These variations may stem from distinct operational conditions governing each chip within the IGBT module. Such phenomenon leads to varying degrees of aging. Furthermore, limitations in the IGBT chip manufacturing process contribute to pronounced discrepancies in the saturation conduction voltage drop among the IGBT chips. Therefore, it is difficult to use a unified standard to characterize the aging of the module.

In conclusion, our approach to predicting the junction temperature of IGBTs does not incorporate aging-related parameters as the inputs to network. Including such parameters would introduce additional complexity in acquiring the input variables. Instead, we gather junction temperature data from multiple IGBT modules of identical types to enhance the accuracy of the predicted junction temperature.

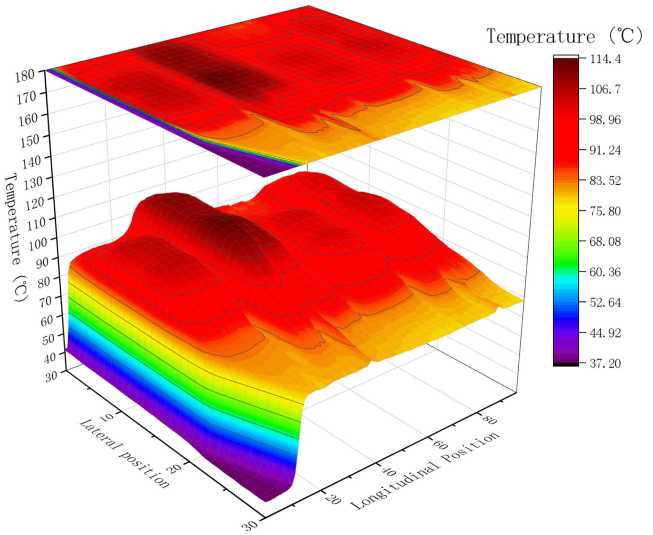

Fig. 16. IGBT junction temperature distribution under Condition 3.

V. Junction Temperature Prediction With Experiment for Verification

A. Experimental Data Acquisition and Conversion

The IGBT module subjected to testing is under various conditions, including different bus voltages, a range of load currents, variable carrier frequencies, and different output electric frequencies. By altering these circuit parameters, the thermal field distribution of the IGBT is obtained. The IGBT static experiments are conducted with the aforementioned parameter variations. After configuring the operating conditions, the IGBT static test circuit is activated, and it is allowed to stabilize. Its operational data, such as the effective value of the output current, output frequency, and heat sink status, are recorded and analyzed.

It is important to provide certain special clarification regarding the thermal imaging data of the IGBT. During the production process of the IGBT module, silicone gel and epoxy glue are used to ensure its electrical insulation and mechanical strength. However, these two materials can reflect ambient light, thereby affecting the acquisition of thermal imaging data. To mitigate this issue, the silicone gel and epoxy glue are removed prior to the experiment, and a uniform coating of black paint is applied onto the module surface. This helps minimize the influence of different materials within the module on thermal imaging. In addition, the black paint provides insulation protection for the IGBT and helps delay oxidation. Before-and-after photos

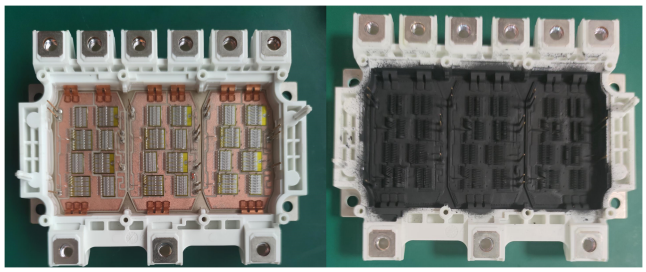

Fig. 17. Experimental module photos before (left) and after (right) processing.

TABLE III
PARAMETERS OF SIMULATION ENVIRONMENT

Items	Configuration
Operating System	Windows11
Deep Learning Framework	MATLAB
Memory	16 GB
MATLAB version	R2023a
CPU	13th Gen Intel(R) i7-13700

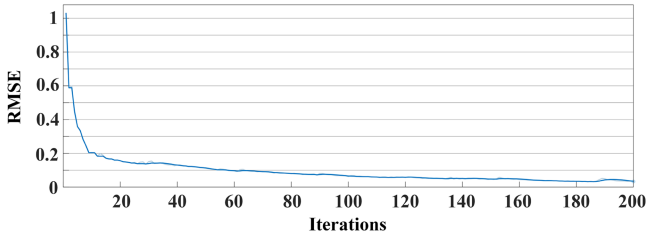

Fig. 18. Curve of the RMSE value during training.

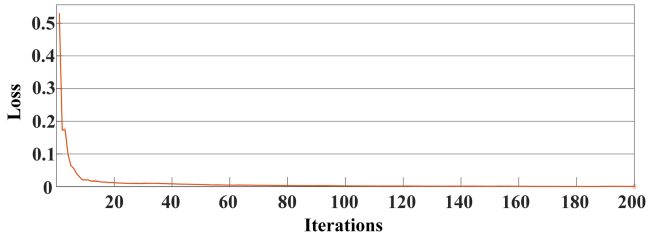

Fig. 19. Curve of the loss function in the experimental tests.

of the experimental module, showing the processing steps, are presented in Fig. 17.

One thermal imaging video of the entire IGBT static test process can be obtained using a thermograph. During the static test, the water tank temperature in the temperature control equipment is set to 65°C with a pressure of 70 kPa and a water flow rate of 7.6L per minute. The experimental data are automatically recorded via video interception, with recording commencing when the IGBT module reaches its maximum temperature of 69.5°C and continuing until the temperature drops back to 69.5°C. The resulting video comprises a dot matrix with a frequency of 20 frames per second. The maximum junction temperature curve of the IGBT is extracted from the thermal imaging video for NN training.

Apart from the hardware experimental facilities described above, we also employ the LSTM NN training to predict the IGBT junction temperature time series, with the training computer parameters listed in Table III.

B. LSTM NN Training

Compared to the CNN network, the LSTM has the advantage of being able to capture the information from both past and future time steps and store the features within the network. In our study, the input and output of LSTM NN trainings utilize IGBT static test circuit parameters and thermal imaging results, respectively. The network input features include the load current, bus voltage, carrier frequency, output frequency, and heat sink related parameters. The network output is the change in the maximum junction temperature of the IGBT over time.

The LSTM prediction is divided into two models. The first model involves the prediction with observed inputs, where the actual results from the previous step are fed into the network before the next prediction. This method is suitable for real-time monitoring with high accuracy. The second method does not require observations, where the training network directly predicts the output based on the given inputs, and it accumulates errors as the length of the prediction sequence increases. This method is suitable for situations where there is no real-time output data, such as providing a reference for packaging and reliability design.

In this section, the LSTM network prediction models with no observed inputs are employed. The training set comprises 6336 sets of IGBT operating parameters, with the first 5696 sets used for training and the remaining 640 sets for validation. The test set consists of 640 data sets not included in the training set. The single-step rolling prediction method is solely utilized in the LSTM network prediction. To obtain multiple forecast outputs, we perform consecutive forecasts while incorporating the previously predicted values. In order to assess the prediction performance of the LSTM networks, we examine three different network hyperparameters: 1) the number of hidden layers, 2) learning rate factor, and 3) the maximum number of epochs. Multiple parameters, such as mean square error (MSE), root-mean-square error (RMSE), and mean absolute error (MAE), are utilized to evaluate the predicted results from the network.

The number of LSTM hidden layers refers to the number of LSTM cells within the training network. Keeping the other parameters in the NN unchanged, as well as the training and test sets, we vary the number of hidden layers to explore its impact on the prediction performance. Specifically, we set the number of hidden layers to 5, 10, 20, 40, 60, 80, 100, 120, and 150. The tested results are presented in Table IV. Therefore, it is evident that the network achieves optimal performance, when the number of hidden layers is set to 100. The corresponding MSE is 0.086265, RMSE is 0.28209, and MAE is 0.2004. In addition, the RMSE of training set reduces to 0.1 after 56 iterations, indicating that the network converges rapidly.

Subsequently, we examine the impact of the learning rate factor on the LSTM network. The learning rate factor determines the adjustment rate of gradient descent during our training. The details of the test data are presented in Table V. In this test, the

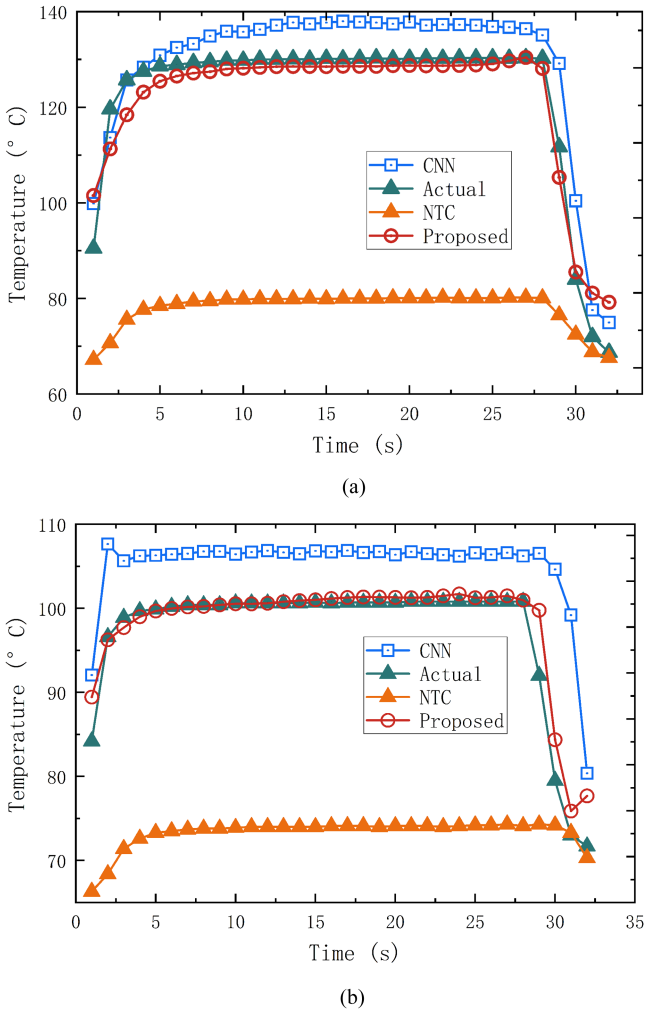

Fig. 20. Performance comparison between the proposed method and the CNN method with different junction temperatures. (a) 130°C. (b) 100°C.

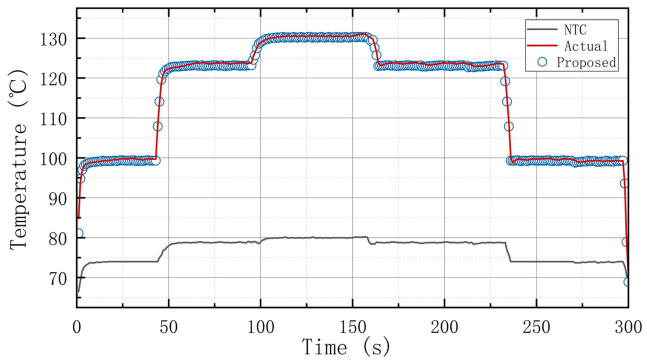

Fig. 21. IGBT operating condition of the predicted results (300 s).

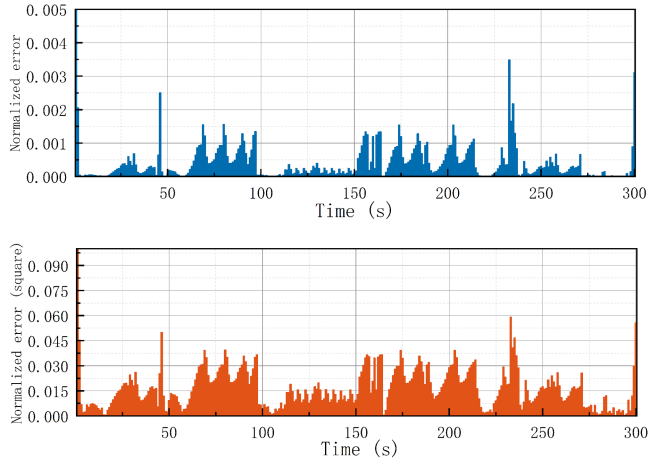

Fig. 22. Error distribution of 300 s IGBT working condition in the predicted results.

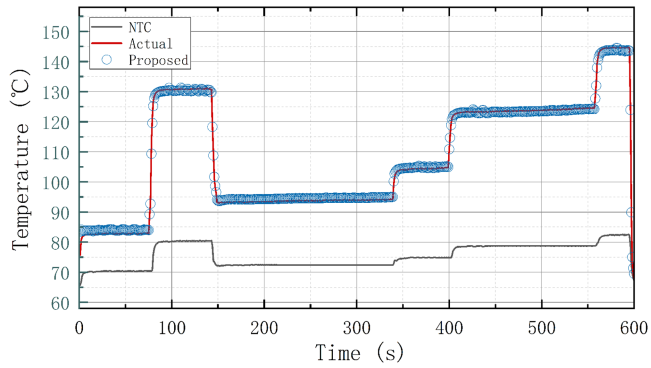

Fig. 23. IGBT operating condition of the predicted results (600 s).

TABLE IV
TESTING SET PERFORMANCE WITH VARIOUS NUMBER OF HIDDEN LAYERS

Number of hidden layers	MSE	RMSE	MAE	RMSE<0.1
5	0.151650	0.36149	0.27335	483
10	0.099756	0.30081	0.19977	224
20	0.132460	0.33472	0.24930	116
40	0.096718	0.30326	0.19142	72
60	0.121300	0.33209	0.24392	58
80	0.101680	0.30374	0.22774	60
100	**0.086265**	**0.28209**	**0.20040**	**56**
120	0.087785	0.28804	0.20345	60
150	0.099032	0.3016	0.22337	64

RMSE<0.1 indicates the number of iterations when the error of training set iteration is just less than 0.1 during the network training; MSE, RMSE, and MAE refer to the error between the predicted result of the test set and the true value.

number of hidden layers is set to 100, and different values of the learning rate factor, namely 0.5, 0.6, 0.7, 0.8, 0.85, and 0.9, are assessed for the LSTM network. From Table V, it can be observed that the network exhibits optimal performance, when the learning rate factor is set to 0.8. Moreover, when the number of hidden layers is fixed at 100, adjusting the learning rate factor has minimal effect on the convergence speed of iterations.

Finally, we investigate the impact of the maximum number of epochs on the LSTM network. The maximum number of epochs refers to the upper limit for the number of training cycles in the LSTM network. In this test, the number of hidden layers is set to 100, the learning rate factor is 0.8, and the maximum number of epochs is varied as follows: 100, 200, 300, 400, 500, 800, 1000,

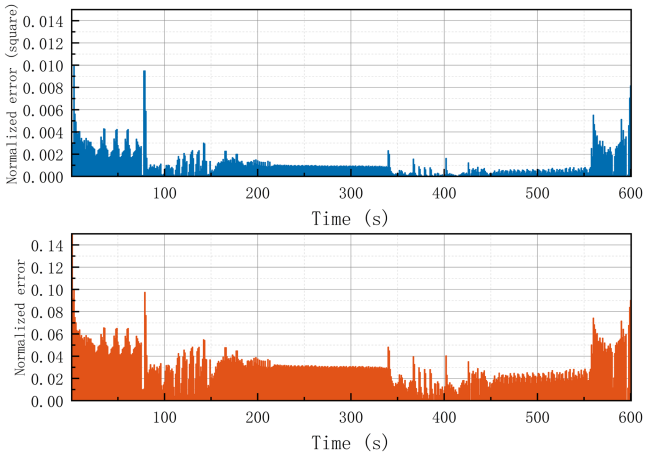

Fig. 24. Error distribution of 600 s IGBT working condition in the predicted results.

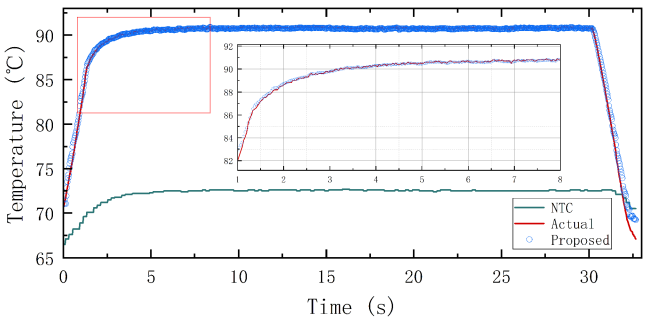

Fig. 25. Predicted results of high sampling frequency under stable junction temperature.

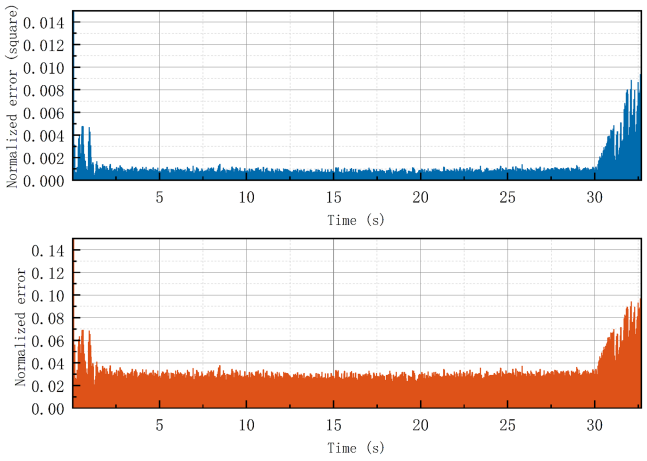

Fig. 26. Error distribution of high sampling frequency in the predicted results under stable junction temperature.

and 2000, respectively. The results of the test are presented in Table VI. The network demonstrates an optimal performance, when the maximum number of epochs is set to 200. Once the hyperparameter values for the LSTM network are determined, the network is trained to fulfill the time series prediction of IGBT junction temperature. A set of optimal prediction results within

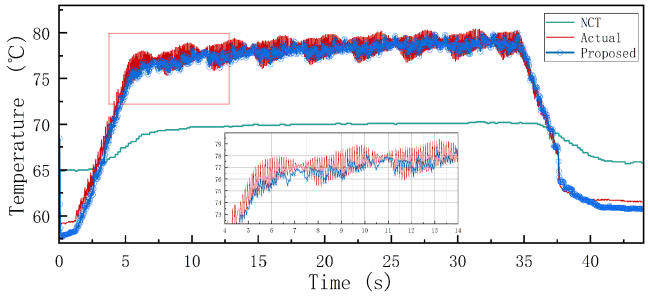

Fig. 27. Predicted results of high sampling frequency under unstable junction temperature.

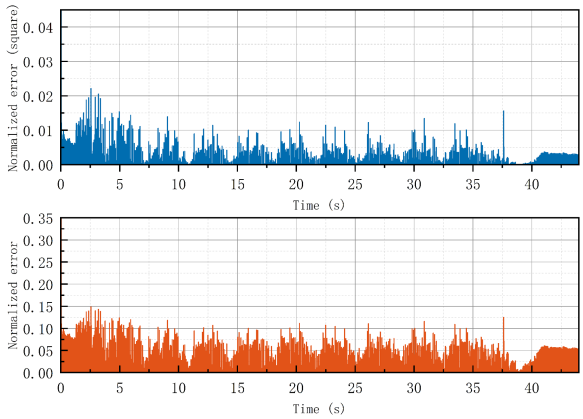

Fig. 28. Error distribution of high sampling frequency in the prediction results under unstable junction temperature.

TABLE V
TESTING SET PERFORMANCE WITH VARIOUS LEARNING RATE FACTORS

Learning rate factor	MSE	RMSE	MAE	RMSE<0.1
0.50	0.126550	0.32717	0.26661	57
0.60	0.099581	0.29730	0.22017	56
0.70	0.117460	0.32030	0.25440	56
0.80	**0.094126**	**0.29382**	**0.21827**	**56**
0.85	0.101160	0.29165	0.23003	54
0.90	0.136000	0.33484	0.25989	55

a fixed dataset can be achieved through fine-tuning various hyperparameters. As the dataset size increases, the network gains deeper feature learning capabilities, effectively mitigating the overfitting.

C. Performance Comparison of the Proposed IGBT Time Series Prediction Method and CNN Method

This subsection verifies the performance of the proposed method for predicting IGBT junction temperature without observed values. At the same time, under the same data set and test set, the predicted effect of LSTM network and CNN network is compared.

As each analysis presented in the previous section, the hyperparameters associated with the LSTM network training are evaluated. In this phase of training, the number of LSTM hidden

TABLE VI
TESTING SET PERFORMANCE WITH VARIOUS MAXIMUM NUMBER OF EPOCHS

Maximum number of epochs	MSE	RMSE	MAE	RMSE<0.1
100	0.101170	0.29246	0.23535	56
200	**0.068732**	**0.25213**	**0.18683**	**57**
300	0.117780	0.32277	0.24112	56
400	0.099288	0.29998	0.22611	58
500	0.111330	0.31308	0.23744	56
800	0.123960	0.32866	0.25879	57
1000	0.089429	0.28455	0.21772	56
2000	0.099235	0.30467	0.21382	58

TABLE VII
PREDICTION ERROR AT HIGH JUNCTION TEMPERATURE INTERVAL

Method	MSE	RMSE	MAE
CNN	1.7369	1.1823	0.2090
Proposed	**0.5667**	**0.5578**	**0.0986**

TABLE VIII
PREDICTION ERROR AT LOW JUNCTION TEMPERATURE INTERVAL

Method	MSE	RMSE	MAE
CNN	2.6836	1.3800	0.2439
Proposed	**0.1640**	**0.2034**	**0.0359**

layers is set to 100, the learning rate factor is 0.8, and the maximum number of epochs is 200. The training dataset consists of 6336 instances of IGBT operating parameters, with the initial 5696 instances being utilized for training and the remaining 640 utilized for validation purposes. Fig. 18 illustrates the curve denoting the variation in RMSE values with the progress of iterations, while the curve depicting the loss can be observed in Fig. 19.

Based on the findings illustrated in Figs. 18 and 19, it can be observed that the RMSE progressively decreases and reaches the value below 0.1 after 60 iterations approximately. Furthermore, the loss function exhibits a noticeable drop within the initial 20 iterations. This phenomenon signifies that the LSTM network possesses the capability to extract relevant features from the training set, and learn the intricate relationship between temperature variations and circuit parameters.

In order to ascertain the predictive effectiveness of the LSTM network for predcting the IGBT junction temperature, we conducted a comparison study by training a CNN network on the same dataset, utilizing identical training and validation sets employed during the LSTM training.

Furthermore, we performed an empirical evaluation of both CNN and LSTM networks on an independent dataset that was excluded from the training set. Fig. 20 portrays the comparison results, wherein "NTC" represents the measured temperature of the thermistor in the IGBT module. It is shown that the proposed method can predict the junction temperature accurately, which agrees the actual data curve very well. However, during instances where there is a sudden rise or fall in temperature, there is a slight discrepancy in the prediction. This quantitative effect can also be drawn from Fig. 20, from which it is clear that the predicted value is very close to the actual one over a period of 5–27 s. Similarly, at temperatures different from 100°C, some degrees of error still persist. In overall, the proposed algorithm exhibits satisfied performance across various working conditions, albeit with a slight deviation when there are abrupt temperature fluctuations.

In order to comprehensively assess the testing process, we divided it into two intervals based on the highest junction temperature values: 110–150°C and 70–110°C. The corresponding errors of the testing sets for these intervals are summarized in Tables VII and VIII, respectively.

As depicted in Tables VII and VIII, the proposed method outperforms CNN networks in both temperature ranges, as evident from the lower error values across all three types of error calculation methodologies. These notable reductions in error substantiate the applicability and efficacy of the LSTM networks for time series prediction of the IGBT junction temperature. Thus, our proposed method holds immense potential for the implementation in real scenarios.

D. Performance of the Proposed IGBT Time Series Prediction Method for Continuous Long-Term Prediction

In the context of the IGBT online prediction NN, the model encompasses a maximum of 43.3 thousand learnable parameters. The training duration for processing 119 394 sets of training data is 5736 s. Running on the device with parameters shown in Table III, the average inference time of the network prediction junction temperature is 0.019 s.

This section aims at evaluating the junction temperature prediction performance of the LSTM network under prolonged IGBT operating conditions using the observed value mode. The predicted results for 300 s consecutive conditions, with a sampling frequency of 1 sample per second, are illustrated in Fig. 21. The error distribution of the predicted results for the continuous 300-s condition is depicted in Fig. 22. In addition, the predicted results and error distribution for the 600-scontinuous IGBT operating conditions are shown in Figs. 23 and 24, respectively.

E. Performance of the Proposed IGBT Time Series Prediction Method for High Sampling Frequency Prediction

This subsection verifies the predicted effect of LSTM network on the change in IGBT junction temperature under the condition of high sampling frequency. The junction temperature is predicted under stable and unstable conditions with a sampling frequency of 30 points per second, respectively. The predicted results under the condition of stable junction temperature are shown in Fig. 25, and the error distribution of the predicted results is shown in Fig. 26. When both the output frequency and the carrier frequency of the modulated signal are very low, the IGBT junction temperature will jitter in a certain interval. The predicted results of IGBT junction temperature instability are shown in Fig. 27, and the error distribution is shown in Fig. 28.

VI. Conclusion

This article presents one LSTM-based method for accurately characterizing the time series of IGBT junction temperature. The training process involves systematically investigating and validating the dependence relationship between experimental parameters and IGBT junction temperature. The measured data are utilized as the training set, while the carefully analyzed parameters serve as the training parameters. Moreover, an extensive exploration of different hyperparameters of NN is conducted for optimizing the deep learning training scheme. The effectiveness of the proposed method is substantiated by comprehensive simulations and experiments.

In particular, the reliability and applicability of such an IGBT junction temperature time series prediction method are demonstrated through successful validation on the specific IGBT modules. On the other hand, it should be noted that as we apply the above method for training the other model, an appropriate retraining and adjustment of the network should be required. We would like to say that our method can not only predict the junction temperature of IGBT in real time but also establish the parameter-dependence verification for the other temperature estimation method.

References

[1] Y. Kang et al., "Research progress in failure mechanism and health state evaluation index system of welded IGBT power modules," *Electronics*, vol. 12, no. 15, Jul. 2023, Art. no. 3248.

[2] S. Yang, A. Bryant, P. Mawby, D. Xiang, L. Ran, and P. Tavner, "An industry-based survey of reliability in power electronic converters," *IEEE Trans. Ind. Appl.*, vol. 47, no. 3, pp. 1441–1451, May/Jun. 2011.

[3] M. H. Nguyen and S. Kwak, "Enhance reliability of semiconductor devices in power converters," *Electronics*, vol. 9, no. 12, Dec. 2020, Art. no. 2068.

[4] L. Dupont, Y. Avenas, and P. O. Jeannin, "Comparison of junction temperature evaluations in a power IGBT module using an IR camera and three thermosensitive electrical parameters," *IEEE Trans. Ind. Appl.*, vol. 49, no. 4, pp. 1599–1608, Jul./Aug. 2013.

[5] Y. Ohsone, G. Wu, and A. Majumdar, "Optical measurement of thermal contact conductance between wafer-like thin solid samples," *J. Heat Transfer*, vol. 121, pp. 954–963, Mar. 1999.

[6] Y. S. Park, H. W. Choi, K. B. Lee, and J. W. Lee, "Thermal estimation of modular multilevel converter submodule using deep regression on GRU and LSTM network," *IEEE Access*, vol. 10, pp. 75343–75353, 2022.

[7] R. Alcala, L. Bhatnagar, and G. Paniagua, "Development of a conduction-free total temperature probe based on the two-wire thermocouple concept," in *Proc. ASME Turbomachinery Tech. Conf. Expo.*, 2023 , vol. 4, pp. 1–10.

[8] Y. Zhou et al., "Dynamic junction temperature estimation via built-in negative thermal coefficient (NTC) thermistor in high power IGBT modules," in *Proc. IEEE Appl. Power Electron. Conf. Expo.*, 2017, pp. 772–775.

[9] M. Ma, X. Yan, W. Guo, S. Yang, G. Cai, and W. Chen, "Online junction temperature estimation using integrated NTC thermistor in IGBT modules for PMSM drives," *Microelectronics Rel.*, vol. 114, Nov. 2020, pp. 113836.

[10] B. Liu, F. Xiao, Y. Luo, Y. Huang, and Y. Xiong, "A multi-timescale prediction model of IGBT junction temperature," *IEEE J. Emerg. Sel. Topics Power Electron.*, vol. 7, no. 3, pp. 1593–1603, Sep. 2019.

[11] K. Górecki and P. Górecki, "Nonlinear compact thermal model of the IGBT dedicated to SPICE," *IEEE Trans. Power Electron.*, vol. 35, no. 12, pp. 13420–13428, Dec. 2020.

[12] J. Li, A. Castellazzi, M. A. Eleffendi, E. Gurpinar, C. M. Johnson, and L. Mills, "A physical RC network model for electrothermal analysis of a multichip SiC power module," *IEEE Trans. Power Electron.*, vol. 33, no. 3, pp. 2494–2508, Mar. 2018.

[13] J. Ye, K. Yang, H. Ye, and A. Emadi, "A fast electro-thermal model of traction inverters for electrified vehicles," *IEEE Trans. Power Electron.*, vol. 32, no. 5, pp. 3920–3934, May 2017.

[14] L. Cao, X. Fan, D. Li, W. Kong, R. Qu, and Z. Liu, "Improved LPTN-based online temperature prediction of permanent magnet machines by global parameter identification," *IEEE Trans. Ind. Electron.*, vol. 70, no. 9, pp. 8830–8841, Sep. 2023.

[15] W. Guo et al., "Real-time average junction temperature estimation for multichip IGBT modules with low computational cost," *IEEE Trans. Ind. Electron.*, vol. 70, no. 4, pp. 4175–4185, Apr. 2023.

[16] S. Gao, K. Ngo, and G. Lu, "Two-dimensional mapping of interface thermal resistance by transient thermal measurement," *IEEE Trans. Ind. Electron.*, vol. 68, no. 5, pp. 4448–4456, May 2021.

[17] L. C. Ordonez, A. D. Exposito, P. A. Cervera, M. Bakic, and T. Wijekoon, "Fast and accurate analytical thermal modeling for planar PCB magnetic components," *IEEE Trans. Power Electron.*, vol. 38, no. 6, pp. 7480–7491, Jun. 2023.

[18] Z. Wang and W. Qiao, "A physics-based improved cauer-type thermal equivalent circuit for IGBT modules," *IEEE Trans. Power Electron.*, vol. 31, no. 10, pp. 6781–6786, Oct. 2016.

[19] J. Chen, S. Yang, and Z. Ren, "A network topological approach-based transient 3-D electrothermal model of insulated-gate bipolar transistor," *IEEE Trans. Magn.*, vol. 56, no. 2, Feb. 2020, Art. no. 7509404.

[20] C. Lv, J. Liu, Y. Zhang, J. Yin, and X. Zhang, "A high-resolution analytical thermal modeling method of capacitor bank considering thermal coupling and different cooling modes," *IEEE Trans. Power Electron.*, vol. 38, no. 6, pp. 7674–7684, Jun. 2023.

[21] R. Shafaei, M. Ordonez, and M. A. Saket, "Three-dimensional frequency-dependent thermal model for planar transformers in LLC resonant converters," *IEEE Trans. Power Electron.*, vol. 34, no. 5, pp. 4641–4655, May 2019.

[22] J. Wang, Z. Qi, Y. Duan, L. Wang, C. Zhao, and F. Yang, "A temperature prediction model of T-type inverter module based on multi-physics coupling," in *Proc. IEEE Int. Power Electron. Appl. Conf. Expo.*, 2018, pp. 1–6.

[23] X. Du, J. Zhang, S. Zheng, and H. M. Tai, "Thermal network parameter estimation using cooling curve of IGBT module," *IEEE Trans. Power Electron.*, vol. 34, no. 8, pp. 7957–7971, Aug. 2019.

[24] M. Akbari, A. Sajjad, M. Bina, B. Eskandari, F. Iannuzzo, and F. Blaabjerg, "A multi-layer RC thermal model for power modules adaptable to different operating conditions and aging," in *Proc. 20th Eur. Conf. Power Electron. Appl.*, 2018, pp. 1–10.

[25] A. Bahman, K. Ma, P. Ghimire, F. Iannuzzo, and F. Blaabjerg, "A 3-D-lumped thermal network model for long-term load profiles analysis in high-power IGBT modules," *IEEE J. Emerg. Sel. Topics Power Electron.*, vol. 4, no. 3, pp. 1050–1063, Sep. 2016.

[26] G. L. Skibinski and W. A. Sethares, "Thermal parameter estimation using recursive identification," *IEEE Trans. Power Electron.*, vol. 6, no. 2, pp. 228–239, Apr. 1991.

[27] K. Wang and Z. Pan, "An analytical model for steady-state and transient temperature fields in 3-D integrated circuits," *IEEE Trans. Compon., Packag. Manuf. Technol.*, vol. 6, no. 7, pp. 1026–1039, Jul. 2016.

[28] L. Choobineh and A. Jain, "An explicit analytical model for rapid computation of temperature field in a three-dimensional integrated circuit (3D IC)," *Int. J. Thermal Sci.*, vol. 87, pp. 103–109, Aug. 2015.

[29] Y. Yang et al., "Thermal–electrical modeling and co-optimization of a half-bridge power module with silver- sintered molybdenum packaging," *IEEE Trans. Power Electron.*, vol. 38, no. 9, pp. 11277–11289, Sep. 2023.

[30] W. Lai et al., "In-Situ calibration method of online junction temperature estimation in IGBTs for electric vehicle drives," *IEEE Trans. Power Electron.*, vol. 38, no. 1, pp. 1178–1189, Jan. 2023.

[31] Y. Kim and S.-K. Sul, "On-line estimation of IGBT junction temperature using on-state voltage drop," in *Proc. Conf. Rec. IEEE Ind. Appl. Conf., 33rd IAS Annu. Meeting*, 1998, vol. 2, pp. 853–859.

[32] U.-M. Choi, S. Jørgensen, and F. Blaabjerg, "Advanced accelerated power cycling test for reliability investigation of power device modules," *IEEE Trans. Power Electron.*, vol. 31, no. 12, pp. 8371–8386, Dec. 2016.

[33] Z. Xu, F. Xu, and F. Wang, "Junction temperature measurement of IGBTs using short-circuit current as a temperature-sensitive electrical parameter for converter prototype evaluation," *IEEE Trans. Ind. Electron.*, vol. 62, no. 6, pp. 3419–3429, Jun. 2015.

[34] P. Sun, C. Gong, X. Du, Q. Luo, H. Wang, and L. Zhou, "Online condition monitoring for both IGBT module and DC-link capacitor of power converter based on short-circuit current simultaneously," *IEEE Trans. Ind. Electron.*, vol. 64, no. 5, pp. 3662–3671, May 2017.

[35] C. H. van der Broeck, A. Gospodinov, and R. W. De Doncker, "IGBT junction temperature estimation via gate voltage plateau sensing," *IEEE Trans. Ind. Appl.*, vol. 54, no. 5, pp. 4752–4763, May 2018.

[36] N. Baker and F. Iannuzzo, "The temperature dependence of the flatband voltage in high-power IGBTs," *IEEE Trans. Ind. Electron.*, vol. 66, no. 7, pp. 5581–5584, Jul. 2019.
[37] H. Luo, Y. Chen, P. Sun, W. Li, and X. He, "Junction temperature extraction approach with turn-off delay time for high-voltage high-power IGBT modules," *IEEE Trans. Power Electron.*, vol. 31, no. 7, pp. 5122–5132, Jul. 2016.
[38] H. Kuhn and A. Mertens, "On-line junction temperature measurement of IGBTs based on temperature sensitive electrical parameters," in *Proc. 13th Eur. Conf. Power Electron. Appl.*, 2009, pp. 1–10.
[39] V. K. Sundaramoorthy, E. Bianda, M. Kamel, G. J. Riedel, and I. Nistor, "Online junction temperature estimation for IGBT modules with paralleled semiconductor chips," in *Proc. 7th IET Int. Conf. Power Electron. Mach. Drives*, 2014, pp. 1–5.
[40] H. Wang et al., "A junction temperature monitoring method for IGBT modules based on turn-off voltage with convolutional neural networks," *IEEE Trans. Power Electron.*, vol. 38, no. 8, pp. 10313–10328, Aug. 2023.
[41] W. Kirchgässner, O. Wallscheid, and J. Böcker, "Estimating electric motor temperatures with deep residual machine learning," *IEEE Trans. Power Electron.*, vol. 36, no. 7, pp. 7480–7488, Jul. 2021.
[42] X. Zeng et al., "A novel virtual sensing with artificial neural network and K-means clustering for IGBT current ceasuring," *IEEE Trans. Ind. Electron.*, vol. 65, no. 9, pp. 7343–7352, Sep. 2018.
[43] D. Herwig, T. Brockhage, and A. Mertens, "Combining multiple temperature-sensitive electrical parameters using artificial neural networks," in *Proc. 22nd Eur. Conf. Power Electron. Appl.*, 2020, pp. 1–10.
[44] C. Dong and P. Mao, "The junction temperature measurement of insulated gate bipolar transistor based on multi-layer feed-forward neural network is presented," in *Proc. IEEE Int. Conf. Mechatron. Automat.*, 2020, pp. 136–140.
[45] Y. Yuan, L. Yunfei, and W. Yang, "Online junction temperature estimation system for IGBT based on BP neural network," in *Proc. IEEE 5th Int. Conf. Electron. Technol.*, 2022, pp. 526–531.
[46] Y. Yang, X. Ding, and P. Zhang, "A novel junction temperature estimation method independent of bond wire degradation for IGBT," *IEEE Trans. Power Electron.*, vol. 38, no. 8, pp. 10526–10268, Aug. 2023.
[47] D. Jyotishi and S. Dandapat, "An LSTM-based model for person identification using ECG signal," *IEEE Sensors Lett.*, vol. 4, no. 8, Aug. 2020, Art. no. 6001904.
[48] Y. Gong, M. Yin, L. Huang, C. Deng, and B. Yuan, "Algorithm and hardware co-design of energy-efficient LSTM networks for video recognition with hierarchical tucker tensor decomposition," *IEEE Trans. Comput.*, vol. 71, no. 12, pp. 3101–3114, Dec. 2022.
[49] J. Ma, H. Liu, C. Peng, and T. Qiu, "Unauthorized broadcasting identification: A deep LSTM recurrent learning approach," *IEEE Trans. Instrum. Meas.*, vol. 69, no. 9, pp. 5981–5983, Sep. 2020.
[50] X. Shi, Z. Chen, H. Wang, and D. Yeung, "Convolutional LSTM network: A machine learning approach for precipitation nowcasting," in *Proc. 29th Ann. Conf. Neural Inf. Process. Syst. (NIPS)*, 2015, pp. 802–810.
[51] J. Donahue et al., "Long-term recurrent convolutional networks for visual recognition and description," *IEEE Trans. Pattern Anal. Mach. Intell.*, vol. 39, no. 4, pp. 677–691, Apr. 2017.
[52] A. Graves, "Generating sequences with recurrent neural networks," 2014, *arXiv:1308.0850v5*.
[53] H. Jiang, F. Qin, J. Cao, Y. Peng, and Y. Shao, "Recurrent neural network from adder's perspective: Carry-look ahead RNN," *Neural Netw.*, no. 144, pp. 297–306, Dec. 2021, *arXiv: 2106.12901*.
[54] M. Caruso and C. Jarne, "Recurrent neural networks as electrical networks, a formalization," in *Proc. 19th Int. Symp. Distrib. Comput. Artif. Intell. (DCAI)*, 2023, no. 585, pp. 105–114.
[55] R. Wen, K. Torkkola, B. Narayanaswamy, and D. Madeka, "A multi-horizon quantile re-current forecaster," 2017, *arXiv:1711.11053*.

Zheng-Wei Du (Student Member, IEEE) received the B.E. degree in engineering and automation from Northeast Electric Power University, Jilin City, China, in 2020, and the M.Eng. degree in electronic information with Harbin Engineering University, Harbin, China, in 2023. He is currently working toward the Ph.D. degree in electronic science and technology with Zhejiang University, Hangzhou, China.

His current research interests include reliability of power semiconductor devices and measurement and simulation of semiconductor devices.

Yu Zhang received the B.E. degree in electronic science and technology from the School of Physics and Electronic, Hunan University, Changsha, China, in 2022. He is currently working toward the master's degree in electronic science and technology with Zhejiang University, Hangzhou, China.

His current research interests include the reliability of high-voltage and high-power electronic devices.

Yuankui Wang received the master's degree in electrical engineering from Jiangsu University, Zhenjiang, China, in 2004. He is currently working toward the Ph.D. degree in ocean engineering technology with Zhejiang University, Hangzhou, China.

Since 2004, he has been with the Kunming Branch of the 705 Research Institute, China State Shipbuilding Corporation, Ltd., Kunming, China, where he is currently a Professor-Level Senior Engineer. His current research interests include PMSM and controller.

Zhiyuan Chen received the B.E. degree in electronic science and technology from Zhejiang University, Hangzhou, China, in 2022. He is currently working toward the master's degree in electronic science and technology with Zhejiang University, Hangzhou, China.

His research interests include the reliability evaluation and temperature management of power semiconductor devices.

Yin-Da Wang (Graduate Student Member, IEEE) received the B.E. degree in information engineering from Nanjing University of Aeronautics and Astronautics, Nanjing, China, in 2020. He is currently working toward the Ph.D. degree in electronic science and technology with Zhejiang University, Hangzhou, China.

His research interests include finite element method, multiphysics modeling, computational electromagnetics, optimization theory, and high-performance computing.

Rui Wu received the B.E. and M.S. degrees in precision instrument and machinery from North University of China, Taiyuan, China, in 2004 and 2007, respectively. He is currently working toward the Ph.D. degree in energy and power engineering with Nanjing University of Aeronautics and Astronautics, Nanjing, China.

He was with Chery Automobile Company, Ltd., from 2007 to 2017, then with Zhejiang Hezhong New Energy Vehicle Company, Ltd., from 2015 to 2018. He is currently the Vice General Manager and Technical Director with Zhejiang Grecon Semiconductor Company, Ltd. His current research interests include design of power semiconductor and electric drive systems for new energy vehicles.

Dongyan Zhao (Senior Member, IEEE) received the B.S. and M.S. degrees in mechanical engineering from the Shanghai Jiao Tong University, Shanghai, China, in 1992 and 1998, respectively. She is currently working toward the Ph.D. degree in electronic information with International College, Zhejiang University, Hangzhou, China.

After ten years with the State Grid Key Laboratory of Power Industrial Chip Design and Analysis Technology, she was appointed as the Director with the Chip Key Lab, Beijing Smart Chip Microelectronics Technology Company Ltd. She was adjunct researcher with Micronano Electronics Department, Zhejiang University, Hangzhou, China. Her research interests include antenna design, chip reliability design, and electromagnetic compatibility.

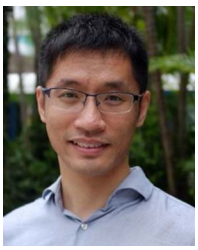

Xin Zhang (Senior Member, IEEE) received the Ph.D. degree in automatic control and systems engineering from the University of Sheffield, Sheffield, U.K., in 2016, and the Ph.D. degree in electronic and electrical engineering from the Nanjing University of Aeronautics and Astronautics, Nanjing, China, in 2014.

From 2017 to 2020, he was an Assistant Professor with Nanyang Technological University. After that, he is currently a Professor with Zhejiang University. His research interests include power electronics, power systems, and advanced control theory, together with their applications in various sectors.

Dr. Zhang is an Associated Editor of many international top journals, such as IEEE TRANSACTIONS ON INDUSTRIAL ELECTRONICS and IEEE JOURNAL OF EMERGING AND SELECTED TOPICS IN POWER ELECTRONICS. He was the recipient of the Highly Prestigious Chinese National Award for Outstanding Students Abroad in 2016.

Wen-Yan Yin (Fellow, IEEE) received the M.Sc. degree in electromagnetic field and microwave technique from Xidian University, Xi'an, China, in 1989, and the Ph.D. degree in electrical engineering from Xi'an Jiaotong University, Xi'an, China, in 1994.

He was an Associate Professor with the Department of Electronic Engineering, Northwestern Polytechnic University, Xi'an, from 1993 to 1996. From 1996 to 1998, he was the Research Fellow with the Department of Electrical Engineering as the AvH scholar, Duisburg University, Duisburg, Germany. From 1998 to 2005, he was with the National University of Singapore as the Research Scientist, Singapore. From 2005 to 2008, he was the Full Professor with the School of Electronic Information and Electrical Engineering, Shanghai Jiao Tong University, Shanghai, China. Since 2009, he has been with the Zhejiang University, Hangzhou, China, as the "Qiu Shi" Distinguished Professor. His current research interests include computational electromagnetic methods and high-performance multiphysics simulation methods and software developments for EMC, 3-D integration, and packaging.